Spatial Correlation and Mobility-Aware Traffic Modeling for Wireless Sensor Networks

Pu Wang, *Student Member, IEEE*, and Ian F. Akyildiz, *Fellow, IEEE, ACM*

***Abstract*—Recently, there has been a great deal of research on using mobility in wireless sensor networks (WSNs) to facilitate surveillance and reconnaissance in a wide deployment area. Besides providing an extended sensing coverage, node mobility along with spatial correlation introduces new network dynamics, which could lead to the traffic patterns fundamentally different from the traditional (Markovian) models. In this paper, a novel traffic modeling scheme for capturing these dynamics is proposed that takes into account the statistical patterns of node mobility and spatial correlation. The contributions made in this paper are twofold. First, it is shown that the joint effects of mobility and spatial correlation can lead to bursty traffic. More specifically, a high mobility variance and small spatial correlation can give rise to pseudo-long-range-dependent (LRD) traffic (high bursty traffic), whose autocorrelation function decays slowly and hyperbolically up to a certain cutoff time lag. Second, due to the *ad hoc* nature of WSNs, certain relay nodes may have several routes passing through them, necessitating local traffic aggregations. At these relay nodes, our model predicts that the aggregated traffic also exhibits the bursty behavior characterized by a scaled power-law decayed autocovariance function. According to these findings, a novel traffic shaping protocol using movement coordination is proposed to facilitate effective and efficient resource provisioning strategy. Finally, simulation results reveal a close agreement between the traffic pattern predicted by our theoretical model and the simulated transmissions from multiple independent sources, under specific bounds of the observation intervals**

***Index Terms*—Long-range dependence, mobility, resource provision, spatial correlation, wireless sensor network (WSN).**

I. Introduction

In THE last few years, a significant number of research efforts have been devoted to the study of developing wide area distributed wireless sensor networks (WSNs) with self-organizing capabilities to cope with sensor node failures, changing environmental conditions, and sensing application diversity [2]. In particular, mobile sensor networks (MSNs) emerge as a promising candidate to support self-organizing mechanisms, enhancing adaptability, scalability, and reliability [3], [10], [17].

Manuscript received May 21, 2009; revised April 28, 2010; October 20, 2010; and March 10, 2011; accepted April 25, 2011; approved by IEEE/ACM TRANSACTIONS ON NETWORKING Editor V. Misra. Date of publication August 08, 2011; date of current version December 16, 2011.

P. Wang is with the Broadband Wireless Networking Laboratory, School of Electrical and Computer Engineering, Georgia Institute of Technology, Atlanta, GA 30309 USA (e-mail: pwang40@ece.gatech.edu).

I. F. Akyildiz is with the School of Electrical and Computer Engineering, Georgia Institute of Technology, Atlanta, GA 30332 USA (e-mail: ian@ece.gatech.edu).

Color versions of one or more of the figures in this paper are available online at http://ieeexplore.ieee.org.

Digital Object Identifier 10.1109/TNET.2011.2162340

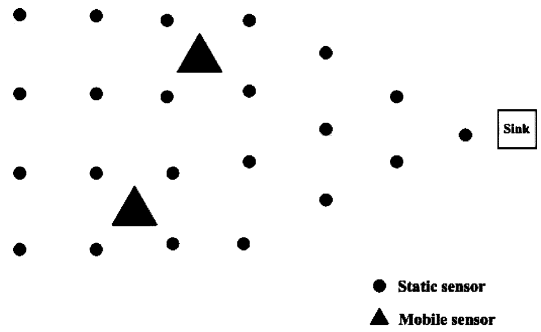

Fig. 1. Hybrid network architecture.

In an MSN, there generally exist two types of nodes: the static sensor nodes, which are deployed in a large area of interests, and mobile agents, which roam around within this area. The mobile agents can retrieve the sensing data from the static sensor nodes and exchange the data with other mobile agents or transmit the data directly to the remote sink. Such a hybrid network scenario, which is illustrated in Fig. 1, facilitates a wide range of civilian and military applications such as battlefield surveillance, nuclear, biological, and chemical attack detection, and environmental monitoring [1]. However, the traffic model in MSNs has not been investigated yet. Conventionally, the Markovian or Constant Bit Rate (CBR) traffic model is generally assumed in WSNs without any discussion as to whether this is appropriate or not. However, since WSNs are an application-specified networking paradigm, different applications or network scenarios can yield different traffic patterns. For example, the WSNs, which are used for intrusion detection and medical applications, can generate traffic significantly different from the conventionally used Poisson or CBR traffic model [8], [15]. Therefore, in this paper, we aim to investigate the influence of two key factors in MSNs, i.e., node mobility and spatial correlation of sensing observations, on the traffic patterns of the mobile nodes. More specifically, we will study whether the joint effects of the two factors induce long-range-dependent (LRD) traffic because such traffic can lead to fundamentally different impact on network performance and protocol design, compared to the traditional Markovian traffic [7], [13], [16].

The seminal work of Leland *et al.* in 1994 [13] established that Ethernet traffic exhibits a property of correlation over many different timescales and suggested that simple LRD models could be applied to effectively capture these correlations. Since then, a great number of research efforts have been devoted to the study of LRD behavior because of the impact of LRD on network performance and resource allocation, which exhibits characteristics significantly different from Markovian traffic. For example, LRD traffic can induce much larger delays than predicted by traditional queuing models. Furthermore, buffering, as a resource allocation strategy, becomes ineffective

with LRD input traffic in the sense of incurring a disproportional penalty in queuing delay compared to the gain in reduced packet-loss probability.

The important consequences of LRD necessitate us to answer the following questions regarding: 1) whether the joint effects of mobility and spatial correlation lead to LRD traffic; and 2) if the answer is yes, how they affect the Hurst parameter that is used to measure the intensity of LRD in the traffic. To answer these questions, we construct an analytical traffic model that incorporates the statistical patterns of node mobility and spatial correlation, and we study the impact of these attributes on traffic statistics, which leads to several novel findings. These findings provide valuable new insights into questions related to the design of efficient and effective protocols for MSNs. The contributions made in this paper include the following.

1) An analytical traffic model is proposed whose parameters are related to the main attributes of MSNs (e.g., mobility and spatial correlation). This model advances an explicit explanation of the impact of these attributes on the statistical patterns of the network traffic.
2) We find that the joint effects of mobility and spatial correlation can lead to pseudo-LRD traffic, whose autocorrelation function approximates that of the LRD traffic with a Hurst parameter up to a certain cutoff time lag.
3) We show that the Hurst parameter of the single-node traffic is closely related to the mobility variability and the degree of spatial correlation. Particularly, higher mobility variability and smaller spatial correlation could give rise to the burstier traffic with larger Hurst parameter. Conversely, lower variance in mobility and larger spatial correlation can lead to nonbursty traffic.
4) We demonstrate that the traffic at the relay node has the same Hurst parameter as the single node, but exhibits much more fluctuations per unit time than the single-node traffic.
5) We propose a novel traffic shaping protocol, which can effectively reduce the traffic burstiness by properly coordinating the movement of the sensor nodes.

From the engineering perspective, one of the emerging applications of this work is battlefield surveillance in tactical networks [1]. In such a type of network, soldiers may roam around within a field of interest, collect information from the static sensor nodes, and execute suitable operations according to the collected information. If the traffic oriented from soldiers is bursty or LRD, without proper network management schemes, this may incur high message delay, serious packet loss, and network congestion. These consequences may jeopardize the precious military assets and degrade information exchange efficiency between military agents. This paper is the first attempt and step toward the effective prediction and evaluation of the traffic nature in this type of network.

In Section II, we introduce background and motivation. Section III presents the proposed traffic modeling scheme, investigates the effects of mobility and spatial correlation on the traffic statistics, and introduces the traffic shaping schemes using movement coordination. Section IV presents experimental results. Finally, Section V provides concluding remarks.

II. Background and Motivation

In this section, we first present the characteristics of MSNs including node mobility and spatial correlation, all of which have significant impact on the traffic nature in MSNs. Then, we outline the motivation behind this work.

A. Node Mobility

Based on different applications, the mobile agent may follow different movement patterns. For example, in battlefield surveillance, the mobile agents could be soldiers, whose mobility behavior can be properly characterized by the human mobility models (Levy walk) [18]. On the other hand, for other applications such as nuclear attack detection, the mobile agents could be robots, and their movement can be controlled or preprogrammed so that they may not follow human movement patterns. However, the key objective of this work is to show that the human mobility pattern, which mobile agents may follow, has a close relationship with the LRD in network traffic. What is more important, the analytical results under the human mobility model also provide valuable guidelines on how to design the effective resource provisioning strategy for WSNs with any type of mobile agents.

The recent seminal work [18] has investigated the human mobility features based on real GPS traces. The data reveal that the statistical pattern of human movements can be characterized by a two-state process alternating between pausing and moving. The distance a human object traveled during the moving state is defined as flight length. The length of a flight is measured by the longest straight-line trip from one location to another that the human object makes without a directional change. The flight length has been revealed to follow heavy-tailed distribution [16]. Accordingly, its survival function can be expressed by

$$\bar{F}_d(x) = P(X \geq x) = \left(\frac{b}{x}\right)^{\alpha}, \qquad x \geq b \tag{1}$$

where X is the flight length, $b \geq 0$ denotes the minimum distance a human agent can travel, and α denotes tail index. According to [18], the tail index will be close to 1 for the outdoor environment. In this case, the human mobility will exhibit high variability since the flight length will drastically fluctuate within a wide range of values over three orders of magnitudes (i.e., 1000 m). This high mobility variability has been shown to be determined by human intentions to travel from one position to another without much deviation caused by geographical constraints such as roads and buildings.

B. Spatial Correlation

Besides node mobility, spatial correlation is another significant characteristic of MSNs. For typical MSN applications, the mobile agents are required to observe the phenomenon of interest at different locations in the field and send the measured data to the sink(s). The observed phenomenon is usually a spatially dependent continuous process, in which the measured data have a certain spatial correlation. In general, the degree of the spatial correlation in the data increases with the decrease of the separation between two observing locations. To quantify the spatial correlation, the observations $S_1, S_2, \ldots, S_N$ at N locations are modeled as an N-dimensional random vector $S = [S_1, S_2, \ldots, S_N]^T$ [5], [19], which has a multivariate normal distribution with $[0, 0, \ldots, 0]^T$ mean and covariance matrix K with each element defined by

$$k_{ij} = \frac{E[S_i S_j]}{\sigma^2}, \qquad i, j = 1, 2, \ldots, N. \tag{2}$$

k_{ij} denotes a correlation function that specifies the correlation model. σ^2 is the variance of each observation S_i. The correlation function is nonnegative and decreases monotonically with the distance $d(i,j)$ between two locations i and j [19].

C. Motivation

As we have seen, MSNs not only inherit the characteristics from conventional WSNs, but also possesses the gene from mobile ad hoc networks (MANETs). The joint effects of these attributes could introduce new dynamics to the network traffic, which are barely observed in conventional static WSNs. These dynamics can be seen in the following aspects.

Mobility along with spatial correlation could lead to temporally correlated traffic. Due to mobility, the data sent in consecutive time slots could be collected at proximal locations. At these locations, the measured data can be highly correlated because of the spatial correlation in the sensed phenomenon. Consequently, the data sent in these consecutive slots have high probability to share similar content. This yields temporal correlation in the network traffic. If this correlation decays slowly as the time lag increases, then the traffic could exhibit LRD behavior. The traffic is called LRD if its autocorrelation function follows a power-law form as the lag approaches infinity

$$\rho(\tau) \to c_p \tau^{\beta-1}, \qquad \text{as } \tau \to \infty \tag{3}$$

where c_ρ is a positive constant and $0 < \beta < 1$ is the fractal exponent. The quantity $H = (\beta+1)/2$ is referred to as the Hurst parameter, which expresses the speed of decay of the autocorrelation function. Note that LRD traffic has slowly decaying autocorrelation function with $0.5 < H < 1$ since $0 < \beta < 1$. By contrast, the short-range-dependent traffic (e.g., Poisson traffic) has fast decaying autocorrelation function (i.e., $\beta > 1$) compared to the LRD traffic.

Previous works [7], [13], [16] have shown that LRD traffic leads to fundamentally different impacts on network performance and protocol design compared to the traditional traffic. To design effective and efficient protocols for MSNs, it is essential to investigate the relationship between the LRD behavior and the dynamics induced by mobility and spatial correlation. Accordingly, we propose a novel traffic modeling scheme that can capture the interplay between the statistical patterns of mobility and spatial correlation. In addition, the statistical analysis of this model is performed to reveal the close relationship between the mobility variability and the bursty nature of the network traffic. These findings provide valuable new insights into questions related to the design of efficient and effective protocols for MSNs.

III. Traffic Modeling for Mobile Sensor Networks

In this section, we propose a structural traffic modeling scheme, which aims to mimic the typical behavior of the mobile node. This scheme is favored because it yields a traffic model whose parameters are related to the traffic generating mechanism and the main attributes of the network (e.g., mobility and spatial correlation). Consequently, it could provide insight into the impact of network design parameters and control strategies on the pattern of the generated traffic. In the rest of this section, we first abstract the behavior of the mobile agent, and then the corresponding traffic model is presented. Based on the proposed model, the statistical analysis is given, and the traffic shaping schemes are proposed.

A. Single-Mobile-Node Traffic

Under this considered network scenario, the behavior of the mobile agent can be described by a procedure having two phases: sensing and transmitting. During the sensing phase, the node moves to a location, executes sensing tasks, and performs in-network data compression. During the transmitting phase, the compressed data are sent at certain rate using suitable transmission mechanisms. This node behavior implies that the pattern of their data transmissions can be naturally characterized by a two-state process that alternates between transmission and silence. According to this abstracted node behavior, we utilize ON/OFF process $X(t)$ to model the single-node traffic, which alternates between two states: the ON state, during which the source transmits data at a rate r, and the OFF state, during which the source is silent. Let $\tau_a(i)$ and $\tau_b(i)$ denote the duration of the ith ON and the ith OFF state, respectively.

The traffic generated by a single sensor node, versus time, can be mathematically modeled as

$$X(t) = \sum_{n=0}^{\infty} r_{[T(n),T(n)+\tau_a(n+1))}(t), \qquad t \geq 0 \tag{4}$$

where $T(n)$ denotes the time of occurrence of the $(n+1)$th ON period, i.e.,

$$T_n = T_0 + \sum_{i=0}^{n} (\tau_a(i) + \tau_b(i)), \qquad n \geq 1$$

and $r_{[T(n),T(n)+\tau_a(n+1))}$ is the indicator function, which is equal to r only for $t \in [T(n), T(n)+\tau_a(n+1))$.

To completely characterize this model, we need to specify the distributions of the ON and OFF periods. The distribution of the OFF period is more affected by the specific sensing operation parameters, such as the sensing time and information processing time. To generalize the analysis, we first assume the OFF period follows any survival function, denoted by $\overline{F_{\tau_b}}(x)$. On the other hand, the ON state distribution, $\overline{F_{\tau_a}}(x)$, depends on the amount of data transmitted at each sensing location. This quantity, which is shown in Section IV-B, is closely related to the statistical features of mobility, spatial correlation, and data rate.

B. Transmission Duration Distribution

Let V denote the file required to be transmitted during an ON period. The length of the ON period τ_a is simply the time to transmit the file using a certain rate r

$$\tau_a = \frac{V}{r}. \tag{5}$$

It is evident that the time for data transmissions depends on the date rates of the specific sensor platforms [1]. For example, the crossbow MICAz nodes equipped with 802.15.4 transceiver modules can achieve up to 250 kps date rate. On the contrary, the crossbow stargate nodes, which leverage 802.11 transceiver modules, can support up to 11 Mps date rate. Without loss of generality, we utilize constant data rate (e.g., $r = 1$). In this

case, the distribution of the ON period length τ_a only depends on the distribution of the file size. To obtain the expression of file size distribution, we first express the file size V in terms of a set of variables related to the network attributes (e.g., spatial correlation and mobility). Then, the probability density function (pdf) of V is derived based on the distributions of these relevant variables.

After the sensor network is deployed, each static sensor node can collect a large number of sensing samples as time proceeds, and then treats n consecutive sensing samples as an event. To preserve the limited memory spaces of the sensors, each sensor is only required to store the smallest collection of events which has probability nearly 1. More specifically, given a predefined small value ε, each sensor only stores the event e that occurs with probability $P(e)$ satisfying

$$2^{-n(H(S)+\varepsilon)} \leq p(e) \leq 2^{-n(H(S)-\varepsilon)}$$

where $H(S)$ is the entropy of the observation S. Accordingly, by the AEP theorem [4], the collection C of such events has probability nearly 1, that is

$$p(C) = \sum_{e \in C} p(e) > 1 - \varepsilon.$$

As ε is made arbitrarily small, the total number of events in the collection C, i.e., the cardinality of C, approximates

$$|C| = 2^{nH(S)}.$$

Obviously, $nH(S)$ bits is sufficient for indexing the events in the collection C. Besides these bits, extra bits are required for conveying more information, such as the source/destination node IDs and the GPS location information of the sensors. Therefore, we assume that the constant number B of bits is used to represent each event. Without loss of generality, we let $B = 1$. Accordingly, the total file size for all events in the collection C approximates

$$V = 2^{nH(S)}. \tag{6}$$

After each movement, a mobile agent retrieves the event information from the closest static sensor node. Intuitively, the spatial proximal static sensor nodes tend to detect and record the same events at the same time instances. Consequently, after each movement, a mobile agent needs to collect and report the previously undetected events, i.e., the events that are different from the ones detected at previous location. More specifically, thanks to the spatial correlation, for a typical event detected at previous location j, at most $2^{nH(S_i|S_j)}$ new events can occur at current location i, where $H(S_i|S_j)$ is the entropy of the observation S_i given the observation S_j. Thus, the number of these new events V reported by the mobile agent at the current location is a function of conditional entropy, which is expressed by

$$V = 2^{nh(S_i|S_j)} = 2^{n(h(S_iS_j)-h(S_j))}. \tag{7}$$

Here, we use differential entropy $h(S_i)$ instead of discrete entropy $H(Si)$ because the observed phenomenon S is generally a continuous random process. Note that the differential entropy differs from discrete entropy by only a constant if the samples are quantized with an identical and sufficient small quantization step. This constant only affects the resolution of quantization and the packet size, but does not change the resulting amount of samples to be transmitted.

We proceed to evaluate the file size V in (7) by adopting the power exponential correlation model, which is a commonly used model in the WSN studies due to its capability of characterizing a wide range of phenomenon [5], [6], [19]. The correlation function of the adopted model is expressed by

$$k = e^{-(\theta_1 d)^{\theta_2}}$$

where d is the mutual distance of two locations. The parameters θ_1 and θ_2 control the correlation level within a given distance d. As a general rule of thumb, a smaller value of θ_1 or θ_2 indicates a higher level of correlation.

Based on the above spatial correlation model, the joint differential entropy of S_i and S_j is given by

$$h(S_iS_j) = \frac{1}{2}\log(2\pi e\sigma^2)^2|K| \tag{8}$$

where K is covariance matrix and $|K|$ is the determinant of K. That is

$$K = \begin{bmatrix} 1 & e^{-(\theta_1 d_{ij})^{\theta_2}} \\ e^{-(\theta_1 d_{ij})^{\theta_2}} & 1 \end{bmatrix}.$$

Inserting (8) into (7), we obtain the closed expression regarding the size of a file conveyed in an ON period

$$V = V_{\max}(1 - e^{-2(\theta_1 d)^{\theta_2}})^{\frac{n}{2}} \tag{9}$$

where $V_{\max} = (2\pi e\sigma^2)^{n/2}$ is the maximum file size, which depends on the properties of the physical phenomenon (e.g., variance σ), and d is the traveled distance or flight length in the preceding OFF period. Equation (9) shows that for a given phenomenon of interest, the file size distribution depends on the distribution of the flight length defined in (1). Accordingly, we obtain the survival function of the file size V

$$\overline{F_v}(x) = (2^{1/\theta_2} b\theta_1)^{\alpha} \left(\ln \left(\frac{V_{\max}^{2/n}}{V_{\max}^{2/n} - x^{2/n}} \right) \right)^{-\alpha/\theta_2} \tag{10}$$

where b is the minimum traveled distance or flight length.

Based on (9), the survival function of the ON period length is given by

$$\overline{F_{\tau_a}}(x) = (2^{1/\theta_2} b\theta_1)^{\alpha} \left(\ln \left(\frac{x_{\max}^{2/n}}{x_{\max}^{2/n} - x^{2/n}} \right) \right)^{-\alpha/\theta_2} \tag{11}$$

where $x \in [x_{\min}\ x_{\max}]$ and $x_{\min} = \left(2\pi e\sigma^2(1 - e^{-2(\theta_1 b)^{\theta_2}})\right)^{n/2}$ and $x_{\max} = (2\pi e\delta^2)^{n/2}$. The pdf of the ON period length is given as

$$f_{\tau_a}(x) = \left(\frac{\alpha b^{\alpha}\theta_1^{\alpha} x}{\theta_2 (V_{\max}^2 - x^2)} \right) \left(\ln \left(\frac{x_{\max}^{2/n}}{x_{\max}^{2/n} - x^{2/n}} \right)^{1/2} \right)^{-\alpha/\theta_2 - 1}. \tag{12}$$

Assuming the minimum file size of 1 and the unit transmission rate ($r = 1$) yields the simplified form of the survival function of the ON period length

$$\overline{F_{\tau_a}}(x) = \left(\ln \frac{x_{\max}^{2/n}}{x_{\max}^{2/n} - 1}\right)^{\alpha/\theta_2} \left(\ln \frac{x_{\max}^{2/n}}{x_{\max}^{2/n} - x^2}\right)^{-\alpha/\theta_2}. \tag{13}$$

Equation (13) shows that the distribution of the ON period length is determined by two factors: the degree of spatial correlation (e.g., θ_2) and mobility variability (e.g., α). Larger θ_2 (or α) indicates a smaller degree of spatial correlation (or smaller mobility variability). To facilitate further analysis, we define the characteristic index as

$$\beta = \frac{\alpha}{n\theta_2}. \tag{14}$$

This index β reflects the joint effect of mobility and spatial correlation that has direct impact on the traffic patterns, which we discuss in detail in the rest of this section.

C. Statistical Analysis

In this section, we derive the autocorrelation function of the single-node traffic. Particularly, we investigate the inherent relationship between the autocorrelation function and network attributes, such as mobility and spatial correlation. The revealed result could point us in new directions for designing efficient and effective protocols for MSNs. These protocols are introduced in the end of this section.

Before evaluating the autocorrelation function, we first investigate the properties of the ON period length, which have a profound impact on the characteristics of the autocorrelation function.

Proposition 1: If the characteristic index $\beta < 1$, then the complementary cumulative distribution function (ccdf) of the ON period $\overline{F_{\tau_a}}(x)$ follows a power-law form with tail index less than 2 within the characteristic region $x \in [x_{\min} \quad x^*]$, where

$$x^* = (2\pi e\sigma^2 R^*)^{n/2}$$

and

$$R^* = \arg\left\{R \middle| \frac{R}{(R-1)\ln(1-R)} = \frac{1}{\beta}\right\} \tag{15}$$

Proof: According to (11), we can express the tail index as

$$\gamma(x) = \frac{d\log \overline{F_{\tau_a}}(x)}{d\log x} = \frac{2\beta x^{2/n}}{x_{\max}^{2/n} - x^{2/n}} \Big/ \ln\left(\frac{x_{\max}^{2/n}}{x_{\max}^{2/n} - x^{2/n}}\right). \tag{16}$$

Equation (16) indicates that the tail index is a function of time x. It is easy to show that $\gamma(x)$ is an increasing function with respect to x because the derivative of the function with respect of x is larger than 0, that is

$$\frac{d\gamma(x)}{dx} = 2x\left(x_{\max}^{2/n} - x^{2/n}\right)\left(\ln \frac{x_{\max}^{2/n}}{x_{\max}^{2/n} - x^{2/n}}\right)^{-2} \geq 0.$$

Therefore, we can obtain the minimum tail index $\gamma_{\min}$ within the region $x \in [x_{\min} \quad x_{\max}]$ by evaluating $\gamma(x)$ at $x_{\min}$. By letting $t = (\theta_1 b)^{\theta_2}$, we have

$$\begin{aligned}\gamma_{\min} &= \gamma(x_{\min}) \\ &= \frac{2\beta(1 - e^{-2(\theta_1 b)^{\theta_2}})}{e^{-2(\theta_1 b)^{\theta_2}} 2(\theta_1 b)^{\theta_2}} \\ &= \frac{2\beta(1 - e^{-t})}{e^{-t} t} \\ &\approx 2\beta(1 + t - 1)/t = 2\beta. \end{aligned} \tag{17}$$

The above approximation holds when t is small, which is the case in the considered network scenario. More specifically, the value of t is determined by θ_1, θ_2, and b. θ_1 and θ_2 control the correlation degree within a given distance. In general, $\theta_2 \in (0, 2]$ and $\theta_1 < 0.1$ are used to model the spatial correlation of the physical event information [19]. On the other hand, b is the minimum traveled distance of the mobile agent. According to [18], this parameter is generally less than 10 m. As a consequence, $t = 2(\theta_1 b)^{\theta_2}$ can approach a small value, and thus (17) holds.

By (17), if $\beta < 1$, then $\gamma_{\min} < 2$. Moreover, since the tail index $\gamma(x)$ in (16) is an increasing function, this implies that there exists a characteristic region of $x \in [x_{\min} \quad x^*]$ such that in this region the tail index $\gamma(x)$ is always less than 2. Therefore, we have the upper bound x^* as follows:

$$x^* = \arg\{x | \gamma(x) = 2\}. \tag{18}$$

To determine x^*, we simplify $\gamma(x)$ in (16) by letting

$$R = (x/x_{\max})^{2/n}$$

and thus we have

$$\gamma(x) = \frac{2\beta R}{(R-1)\ln(1-R)}. \tag{19}$$

By letting $\gamma(x) = 2$, we can obtain R^* as a function of β, i.e.,

$$R^* = \arg\left\{R \middle| \frac{R}{(R-1)\ln(1-R)} = \frac{1}{\beta}\right\}.$$

According to (18), we obtain the upper bound

$$x^* = (2\pi e\sigma^2 R^*)^{n/2}. \tag{20}$$

Based on numerical results, it is easy to show R^* decreases as β increases. More specifically, $R^* \approx 0.7$ for $\beta = 0.5$, while R^* approaches 0 as β approaches 1. □

Proposition 1 shows that the distribution of the ON period length displays different behavior within different regions. If $x \in [x_{\min} \quad x^*]$, then the survival function decays slowly. The decay speed is completely controlled by β or the joint effects of spatial correlation degree α and mobility variability β. By contrast, the survival function of the ON period length decays fast if $x > x^*$. This implies that the ON period distribution can be closely approximated by a mixture model.

Proposition 2: If correlation index $\beta < 1$, the $\overline{F}_{\tau_a}(x)$ can be approximated by mixture Pareto-exponential distribution

$$\overline{F^*_{\tau_a}}(x) = \begin{cases} 1, & 0 \le x < k_1 \\ k_1^{\gamma_a} x^{-\gamma_a}, & k_1 \le x < k_2 \\ \mu e^{-\lambda x}, & k_2 \le x \le k_3 \\ 0, & x > k_3 \end{cases} \tag{21}$$

where $\gamma_a < 2$. $k_1 = x_{\min}$ and $k_3 = x_{\max}$ indicate the lower and upper bounds of the possible length of the ON period, respectively. $k_2 = x^*$ is the upper bound of the characteristic region defined in Proposition 1.

Proof: See Appendix B. □

Proposition 2 states that the ON period length follows power-law (hyperbolic) form within the region $x_{\min} < x < x^*$. Obviously, if x^* is large enough, then ON period length approaches heavy-tail distribution. This actually characterizes the zero frequency behavior (see Appendix A for more details). However, due to the boundary of x^*, the middle frequency behavior of the single-node traffic is of interest, which is further explained in Proposition 3.

Based on the approximated survival function defined in (21), we proceed to derive the autocorrelation function of the single-node traffic. To express the result in a closed form, we need to specify the survival function of the OFF period. To generalize the analysis, we assume that the OFF period follows Pareto distribution so that the OFF period can exhibit a wide range of variability by adjusting the corresponding parameters. The pdf of the OFF period τ_b is expressed by

$$f_{\gamma_b}(x) = \gamma_b m^{\gamma_b} x^{-(\gamma_b+1)} \tag{22}$$

where m denotes the minimum OFF time and γ_b denotes the tail index which controls the variability of OFF interval. Values of γ_b smaller than unity induce OFF durations with infinite mean, whereas values of γ_b exceeding 2 ensure finite variance. In the range of $1 < \gamma_b < 2$, the OFF period lengths have finite mean but exhibit wild variation about that mean as a result of the infinite variance in that range. In sum, the variability of the OFF period increases as γ_b decreases. In addition, to simplify the analysis, we consider the case in which the OFF period is dominated by the time for sensing and information processing, thus implying that the OFF and ON period lengths are independent. To obtain the autocorrelation function, we first investigate the properties of the power spectrum density (PSD).

Proposition 3: If $0.5 < \beta < 1$ 1 and $\gamma_b > 2$, the power spectrum density $S(f)$ of $X(t)$ exhibits power-law decay behavior with fractal exponent $2 - \gamma_a$ in mid-frequency range $k_2^{-1} \ll f \ll k_1^{-1}$

Proof:

1) Mid-Frequency Approximation: Based on the power spectrum density of an ON/OFF process with unit amplitudes and arbitrary distributions of ON and OFF period lengths [14], the power spectrum density of the random process defined by (4) is given by

$$S(\omega) = r^2 E[X(t)]\delta\left(\frac{\omega}{2\pi}\right) + \frac{2r^2(\omega)^{-2}}{E[\tau_a]+E[\tau_b]} \mathrm{Re}\left\{\frac{[1-\varphi_{\tau_a}(\omega)][1-\varphi_{\tau_b}(\omega)]}{1-\varphi_{\tau_a}(\omega)\varphi_{\tau_b}(\omega)}\right\} \tag{23}$$

where $\varphi_{\tau a}$ and $\varphi_{\tau b}$ are the characteristic functions associated with the distributions for ON period length τ_a and OFF period length τ_b, respectively. Based on the survival function of τ_a given in (21), we can get the characteristic function of τ_a given as

$$\begin{aligned} \varphi_{\tau_a}(\omega) &= \int_{k_1}^{k_2} e^{-j\omega x} \gamma_a \frac{k_1^{\gamma_\alpha}}{x^{\gamma_a+1}} dx \\ &\quad + \int_{k_2}^{k_3} e^{-j\omega x} \mu(\lambda e^{-\lambda x} + \delta(x-k_3) e^{-\lambda k_3}) dx \\ &= \gamma_a (j\omega k_1)^{\gamma_a} \int_{j\omega k_1}^{j\omega k_2} e^{-x} x^{-(\gamma_{a+1})} dx \\ &\quad + \frac{\lambda\mu}{j\omega+\lambda} e^{-(j\omega+\lambda)k_2} + \frac{j\omega\mu}{j\omega+\lambda} e^{-(j\omega+\lambda)k_3}. \end{aligned} \tag{24}$$

Since $k_3^{-1} < k_2^{-1} \ll f \ll k_1^{-1}$, we have $k_1/k_2 \to 0$, $\omega k_2 \to \infty$, and $\omega k_3 \to \infty$. Letting $j\omega k_1 = z$, we can obtain

$$\begin{aligned} 1 - \phi_{\tau_a}(\omega) &= \gamma_a (j\omega k_1)^{\gamma_a} \int_{j\omega k_1}^{j\omega k_2} (1 - e^{-x}) x^{-(\gamma_a+1)} dx \\ &\quad + \left(\frac{k_1}{k_2}\right)^{\gamma_a} + \frac{\lambda\mu}{j\omega+\lambda} e^{-(j\omega+\lambda)k_2} \\ &\quad + \frac{j\omega\mu}{j\omega+\lambda} e^{-(j\omega+\lambda)k_3} \\ &\to \alpha z^{\gamma_a} \int_z^{\infty} (1 - e^{-x}) x^{-(\gamma_a+1)} dx. \end{aligned} \tag{25}$$

Since $0.5 < \beta < 1$, we have $1 < \gamma_a < 2$. Then, the expansion of above integration around the origin of z is given by [14]

$$\begin{aligned} Q(x) &= \gamma_a z^{\gamma_a} \int_z^{\infty} (1 - e^{-x}) x^{-(\gamma_a+1)} dx \\ &\to \frac{\gamma_a}{\gamma_a - 1} z - (\gamma_a - 1)^{-1} \Gamma(2 - \gamma_a) z^{\gamma_a}. \end{aligned} \tag{26}$$

We therefore obtain the characteristic function of τ_a

$$\varphi_{\tau_a} \to 1 - \varsigma_1 j\omega + \varsigma_2 (j\omega)^{\gamma_a} \tag{27}$$

where

$$\begin{aligned} \varsigma_1 &= (k_1\gamma_a)/(\gamma_a - 1) \\ \varsigma_2 &= (\gamma_a - 1)^{-1} \Gamma(2 - \gamma_a) k_1^{\gamma_a}. \end{aligned} \tag{28}$$

Because the OFF period length τ_b follows Pareto distribution with minimum value of m and the tail index $\gamma_b > 0$, following the same procedures as above, we can obtain the characteristic function of τ_b given as

$$\varphi_{\tau_b}(\omega) = \int_m^{\infty} e^{-j\omega x} \gamma_b \frac{m^{\gamma_b}}{x^{\gamma_b+1}} \to 1 - \rho_1 j\omega + \rho_2 (j\omega)^{\gamma_b} \tag{29}$$

where

$$\begin{aligned} \rho_1 &= (m\gamma_b)/(\gamma_b - 1) \\ \rho_2 &= (\gamma_b - 1)^{-1} \Gamma(2 - \gamma_b) m^{\gamma_a}. \end{aligned} \tag{30}$$

Inserting (27) and (29) into (23), the latter part of the second term of (23) becomes

$$\begin{aligned}\Omega(\omega) &= \mathrm{Re}\left\{\frac{[1-\varphi_{\tau_a}(\omega)][1-\varphi_{\tau_b}(\omega)]}{1-\varphi_{\tau_a}(\omega)\varphi_{\tau_b}(\omega)}\right\} \\ &= \mathrm{Re}\left\{\frac{\varsigma_1\rho_1\omega^2 - \varsigma_2\rho_1(j\omega)^{\gamma_a+1} - \varsigma_1\rho_2(j\omega)^{\gamma_b+1}}{(\varsigma_1+\rho_1)j\omega - \varsigma_2(j\omega)^{\gamma_a} - \rho_2(j\omega)^{\gamma_b}}\right\} \\ &= -\frac{\varsigma_2\rho_1^2\cos(\frac{\pi}{2}\gamma_a)}{(\varsigma_1+\rho_1)^2}\omega^{\gamma_a} - \frac{\rho_2\varsigma_1^2\cos(\frac{\pi}{2}\gamma_b)}{(\varsigma_1+\rho_1)^2}\omega^{\gamma_b}. \quad (31)\end{aligned}$$

Based on the survival function of τ_a given in (21), we can obtain the mean of τ_a

$$\begin{aligned}E[\tau_a] &= \int_{k_1}^{k_2}\gamma_a x\frac{k_1^{\gamma_a}}{x^{\gamma_a+1}}dx \\ &\quad + \int_{k_2}^{k_3} x\mu(\lambda e^{-\lambda x} + \delta(x-k_3)e^{-\lambda k_3})dx \\ &= \frac{\gamma_a}{\gamma_a-1}\left(k_1 - k_2\left(\frac{k_1}{k_2}\right)^{\gamma_a}\right) \\ &\quad + \left(k_2\mu + \frac{\mu}{\lambda}\right)e^{-\lambda k_2} - \frac{\mu}{\lambda}e^{-\lambda k_3}. \quad (32)\end{aligned}$$

Based on the survival function of Pareto distribution, we can obtain the mean of τ_b

$$E[\tau_b] = \frac{\gamma_a}{\gamma_a-1}m. \quad (33)$$

Inserting (31)–(33) into (23), we can obtain the mid-frequency approximation of the power spectrum density with $k_2^{-1} \ll f \ll k_1^{-1}$

$$S(\omega) = C_1\omega^{\gamma_a-2} + C_2\omega^{\gamma_b-2} \quad (34)$$

where

$$C_1 = -\frac{2(\gamma_a-1)^{-1}\Gamma(2-\gamma_a)k_1^{\gamma_a}\left(\frac{m\gamma_b}{\gamma_b-1}\right)^2 r^2\cos\left(\frac{\pi}{2}\gamma_a\right)}{(E[\tau_a]+E[\tau_b])\left(\frac{k_1\gamma_a}{\gamma_a-1}+\frac{m\gamma_b}{\gamma_b-1}\right)^2} \quad (35)$$

and

$$C_2 = -\frac{2(\gamma_b-1)^{-1}\Gamma(2-\gamma_b)m^{\gamma_b}\left(\frac{k_1\gamma_a}{\gamma_a-1}\right)^2 r^2\cos\left(\frac{\pi}{2}\gamma_b\right)}{(E[\tau_a]+E[\tau_b])\left(\frac{k_1\gamma_a}{\gamma_a-1}+\frac{m\gamma_b}{\gamma_b-1}\right)^2}. \quad (36)$$

Because $\tau_b > 2$ and $\gamma_a \approx 2\beta < 2$, the spectrum density has a fractal exponent $2-2\beta$ in mid-frequency.

2) High-Frequency Approximation: If $\omega \to \infty$, we can obtain the characteristic functions of ON and OFF periods, respectively

$$\varphi_{\tau_a}(\omega) \to 0; \varphi_{\tau_b}(\omega) \to 0.$$

Inserting above equations into (23), we can obtain the asymptotic form of the power spectrum density in the high-frequency limit

$$S(\omega) = \frac{2r^2(\omega)^{-2}}{E[\tau_a]+E[\tau_b]}. \quad (37)$$

3) Low-Frequency Approximation: If $\omega \to 0$, we can obtain the characteristic functions of ON and OFF periods, respectively

$$\varphi_{\tau_a}(\omega) \to 0; \varphi_{\tau_b}(\omega) \to 1 - \rho_1 j\omega + \rho_2(j\omega)^{\gamma_b}$$

Inserting the above equations into (23), we can obtain the asymptotic form of the power spectrum density in the low-frequency limit

$$\begin{aligned}S(\omega) &= \frac{2r^2(\omega)^{-2}}{E[\tau_a]+E[\tau_b]}\mathrm{Re}\{1-\varphi_{\tau_a}(\omega)\} \\ &= \frac{-2r^2(\gamma_b-1)^{-1}\Gamma(2-\gamma_b)m^{\gamma_b}\cos\left(\frac{\pi}{2}\gamma_b\right)}{E[\tau_a]+E[\tau_b]}\omega^{\gamma_b-2} \quad (38)\end{aligned}$$

□

Proposition 3 states that the spectrum density follows power-law form in mid-frequency. According to the relationship between spectrum density and autocorrelation, we can obtain the hyperbolic autocorrelation function within a certain region.

Proposition 4: If $0.5 < \beta < 1$ and $\gamma_b > 2$, the autocorrelation function of the process $X(t)$, denoted by $R(\tau)$, follows the power-law form

$$R(\tau) = D_1 t^{1-\gamma_a} + D_2 t^{1-\gamma_b}$$

in the region $k_1 < |\tau| < k_2$ with some constants D_1 and D_2. The corresponding Hurst parameter is given by

$$H \approx \frac{3-\gamma_a}{2}.$$

Proof: See Appendix C □

Proposition 4 suggests that the joint effects of mobility and spatial correlation can lead to pseudo-LRD traffic, which has power-law autocorrelation function with the Hurst parameter up to the cutoff time lag x^*. This result is important because when x^* is large enough, pseudo-LRD traffic exhibits similar behavior as the LRD traffic, thus demanding similar resource allocation approaches. In addition, Proposition 4 shows that index β completely controls the value of the Hurst parameter and thus has direct impact on the burstiness of the traffic from each mobile agent. This means that the network traffic can exhibit different degrees of burstiness under different monitored environments (e.g., spatial correlation) and node behavior (e.g., mobility variability).

D. Relay-Node Traffic Model

The discussion above has analyzed the traffic pattern of the single mobile node. Due to the nature of *ad hoc* communication in MSNs, there always exist some nodes that act as the relay points responsible for forwarding traffic for other nodes. Next, we turn our attention to the traffic pattern on the relay nodes. For certain relay nodes, there may exist several routes passing through them, each route corresponding to a traffic flow originating from other node. Thus, at each relay node, the traffic flow is the aggregation of all the flows that need to be forwarded. The number of flows actually traversing the relay node is changing over time due to the time-varying topology induced by the mobility nature of MSNs. Suppose within a certain time interval T

each forwarding flow passes through the relay node with an identical and independent probability of $P_{\rm t}$, which is called the traversing probability. Under this condition, the number of active flows N follows binomial distribution. Then, the traffic on the relay node, denoted by $S(t)$, becomes the sum of the traffics of all the active flows during a certain time interval T

$$S(t) = \sum_{n=1}^{N} X_n(t) \tag{39}$$

where $X_n(t), i = 1 \ldots N$ denotes the traffics of active flows, which are independent identically distributed. Suppose the maximum number of flows a relay node can forward is M, which is determined by system parameters such as bandwidth. We turn now to an analysis of the aggregated traffic by examining the statistics of this sum process. We begin by deriving the pdf of the process.

The marginal distribution of a single-flow traffic defined by (4) follows a Bernoulli form

$$P_f = P(X(t) = 1) = E[X(t)] = \frac{E[\tau_a]}{E[\tau_a] + E[\tau_b]}.$$

Since the ON/OFF event of a single flow is independent of the relay node selection of this flow, the number of active flows traversing a relay node is independent of the traffic patterns of these active flows. As a consequence, the distribution of the resulting sum process in (39) follows

$$P(S(t) = n) = \sum_{i=n}^{M} \binom{i}{n} \binom{M}{i} P_f^n (1-P_f)^{i-n} P_t^i (1-P_t)^{M-i} \tag{40}$$

where M is the maximum number of flows a relay node can forward, and P_t is the traversing probability. We now investigate the dependency structure of the aggregation traffic $S(t)$ by examining its autocovariance.

Proposition 5: The traffic at the relay node has Hurst parameter $H \approx (3 - 2\beta)/2$ in the region $k_1 < t < k_2$ with scaled hyperbolic autocovariance as the single flow traffic.

Proof: Taking advantage of the independence of the active flow traffics and the properties of iterative mean, we can obtain

$$\begin{aligned} R_S(\tau) &= E\left[\sum_{i=1}^{N} X_n(s) \sum_{j=1}^{N} X_m(s+\tau)\right] \\ &= E\left[E\left[\sum_{i=1}^{N} X_n(s) \sum_{j=1}^{N} X_m(s+\tau) | N\right]\right] \\ &= E[N R_X(\tau) + N(N-1) E^2[X(t)]] \\ &= M P_t R_X(\tau) + \left(M^2 P_t^2 - M P_t^2\right) E^2[X(t)]. \end{aligned} \tag{41}$$

Based on the relationship between autocorrelation and autocovariance, we obtain

$$\begin{aligned} C_S(\tau) &= R_S(\tau) - E^2[S(t)] \\ &= M P_t R_X(\tau) + (M^2 P_t^2 - M P_t^2) E^2[X(t)] - E^2[S(t)] \\ &= M P_t C_X(\tau) + M\left(P_t - P_t^2\right) E^2[X(t)] \end{aligned} \tag{42}$$

where $C_X(t)$ is the autocovariance of a single traffic flow. Equation (42) indicates that the aggregated traffic on the relay node has the scaled autocovariance of the single traffic flow. In addition, the variance of $S(t)$ is given by

$$\mathrm{Var}[S(t)] = M P_t \sigma_X^2. \tag{43}$$

We obtain the autocorrelation function of $S(t)$, which has the some form as single-flow traffic $X(t)$

$$\rho_S = \frac{C_S(\tau)}{\mathrm{Var}[S(t)]} \approx \frac{C_X(\tau)}{\mathrm{Var}[X(t)]}$$

when the time lag τ is large. Thus, the relay-node traffic has the same Hurst parameter $H \approx (3-2\beta)/2$ as the single-flow traffic. □

Proposition 5 states that the statistics of relay-node traffic closely resemble those of the traffic originating from a single user. Because the aggregated traffic exhibits all of the transitions occurring within each individual traffic flow passing through the relay node, the traffic on the relay node exhibits $M_P(t)$ times more fluctuations than each of the traversing traffic flow.

E. Useful Findings and Intuitive Explanations

Based on the statistical analysis given above, we have two major findings. First, higher mobility variability (smaller α) along with smaller spatial correlation (larger θ_2) could lead to more bursty traffic (higher H). Second, the joint effect of the mobility and correlation could lead to nonbursty traffic (e.g., $H = 0.5$) if a certain condition holds (e.g., $\beta = 1$). The intuitive explanation for these findings is that both higher mobility variability and smaller spatial correlation encourage larger file sizes, thereby increasing the tail weight of the size distribution. This in turn leads to a greater chance to have burst transmissions. Therefore, it can be seen that the traffic burstiness actually arises from the joint effect of node mobility and spatial correlation on the file size, which can be explained as follows. Higher mobility variability indicates higher probability that a node travels a long distance, which means the observation at the current location has little correlation with the previous location. Therefore, at the current location, the sensor node has to transmit a large data file consisting of almost all the gathered information (e.g., images and videos). On the other hand, small spatial correlation implies that the sensing data retrieved at the current location may be completely different from the proximal location. As a result, the sensor node may also need to send a large file of data even though it only travels a short distance. In summary, higher mobility variability along with smaller spatial correlation could lead to higher probability for a node to transmit a large file in the bursty fashion.

F. Traffic Shaping Protocols Using Movement Coordination

These novel findings revealed in this paper point us in new directions for solving the traffic engineering problems. Instead of passively observing the traffic and designing the resource allocation schemes accordingly, new traffic shaping protocols can be proposed to actively shape the traffic so that the resulting traffic can follow the desired characteristics. Then, the existing traffic management schemes can be directly employed accordingly. In our case, due to the direct connection between mobility pattern and the traffic attributes, we can effectively reduce the burstiness of traffic flows by adaptively coordinating

the movement of the sensor nodes so that the protocols designed for smooth or SRD traffic can be employed in more a dynamic network environment such as an MSN.

The proposed traffic shaping protocols are briefly described as follows. 1) If the correlation model of the monitored phenomenon is unknown, then the best effort to reduce the traffic burstiness is to let each mobile node move evenly in the sensing area so that the resulting Hurst parameter is minimized by maximizing α. 2) If the correlation structure (e.g., θ_2) of the monitored phenomenon can be estimated in advance, the node may be allowed to move in a more random manner as long as the mobility variability does not exceed a certain threshold, in which case, α should be always larger than θ_2 so that $\alpha/\theta_2 > 1$. To show the effectiveness of the proposed schemes, next we investigate the queueing performance on the relay node and demonstrate how the proposed scheme simplifies the resource provisioning strategy.

It is easy to prove that if the number of the traversing flows on the relay node is large enough, then the relay node traffic, defined in (39), converges to a fractional Gaussian process [21]. Accordingly, the aggregate cumulative packet traffic follows fractional Brownian motion, which results in Weibull-like asymptotic tail probabilities for queue-length distribution [7], i.e.,

$$P(Q > x) \approx \exp(-\delta x^{2-2H}) \tag{44}$$

where δ is a constant. It is shown in [11] that the slowly decaying tail probabilities given in (44) can result in the "buffer ineffectiveness" phenomenon, in which increasing the buffer sizes beyond a certain value results in only a slight decrease in loss rates. The conventional approach to solve this problem is to utilize a small buffer capacity/large bandwidth resource provisioning strategy, which can curtail the influence of LRD traffic on queueing by keeping buffer capacity small and increasing bandwidth. However, for the bandwidth constraint WSNs, this strategy is infeasible. In this case, selecting the proper traffic shaping protocols under different conditions can boost the queueing performance and simplify the design of resource provisioning strategy.

1) If the spatial correlation degree θ_2 is known, the distance that the mobile agents will travel can be drawn from a distribution that exhibits hyperbolic tails with properly selected tail index α so that the characteristic index $\beta = 1$. Since $H = (3 - 2\beta)/2$ based on Proposition 4, the tail probabilities defined in (44) become asymptotically exponential, e.g.,

$$P(Q > x) \approx \exp(-\delta x) \tag{45}$$

which means that the simple buffering strategy can be used to effectively reduce the loss rates by properly increasing the buffer size.

2) If the spatial correlation degree θ_2 is unknown, the distance the mobile agents will travel can be programmed to follow any distribution with low variability such as the exponential distribution, e.g.,

$$\overline{F_d}(x) = \exp(-\lambda x) \tag{46}$$

where $1/\lambda$ is the average flight length. By combining (9) and (46), the survival function of the ON period length with unit transmission rate can be expressed by

$$\overline{F_{\tau_a}}(x) \approx \exp(-\eta x^{2/\theta_2})\ x \geq 0 \tag{47}$$

where η is a constant and $\eta = \lambda(2)^{-1/\theta_2}/\theta_1$. Equation (47) indicates that ON period does not follow heavy-tail distribution because it decays faster than exponential (e.g., $1 < \theta_2 < 2$). It is known (e.g., see [12]) that if the arrival process is a single ON/OFF source in which the ON periods are exponentially distributed, then the queue length distribution decays exponentially. This means that the simple buffering scheme for SRD traffic can be effectively applied.

Besides enabling the simple resource provisioning strategy, the proposed traffic shaping protocols can improve network performance. Suppose the queue of the relay node is only fed by one traffic flow originating from a single node. Since the ON period defined in (21) approaches heavy-tail distribution as x^* becomes large enough, this leads to the hyperbolic queue-length distribution that decreases more slowly than a Weibull distribution. This could give rise to an infinite mean waiting time, which results in unreasonably large delays. By coordinating the movement of the sensor nodes, the variability of the ON period length is reduced so that the ON period distribution decays faster than heavy-tail distribution. This leads to finite mean waiting time, thus significantly reducing the network latency.

IV. Simulation Results

In this section, we test the validity of the proposed model through simulations and investigate the effects of the mobility and spatial correlation on the traffic patterns through the simulated results.

A. Simulation Parameters

Unless otherwise specified, the simulation parameters are set as follows. The network size is set as $10\,000 \times 10\,000$. The tail index of flight length α is set to be 1.2, which is a typical setting for human mobility pattern in outdoor environment. For the spatial correlation model, the correlation coefficient θ_2 is set to be 2, which indicates the correlation $\beta < 1$ by letting $n = 1$. The minimum duration of the OFF period is 1 s. The tail index of OFF period length is larger than 2. This setting guarantees that the traffic pattern of a single node only depends on the statistical features of the ON period, which further makes traceable the impact of mobility and spatial correlation on the nature of the network traffic. The minimum and maximum file size is 1 and 2000, respectively. In addition, in the multiple-flow case, we assume the maximum number of flows a relay node can support is 20.

B. Estimators of Hurst Parameter

The following two methods are used to estimate Hurst parameter in order to measure the traffic burstiness. The first method is the variance-time plot. The estimate for Hurst parameter can be obtained by proceeding as follows. Express a user's traffic trace by the time sequence $X = \{X_t, t \geq 1\}$, then construct

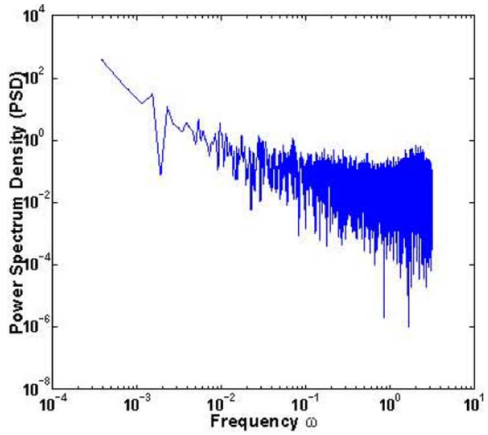

Fig. 2. Estimated PSD.

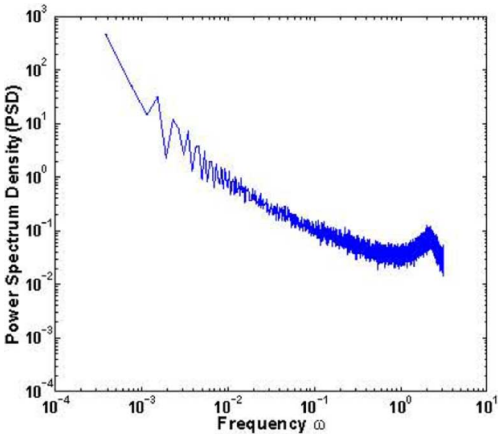

Fig. 3. Averaged PSD.

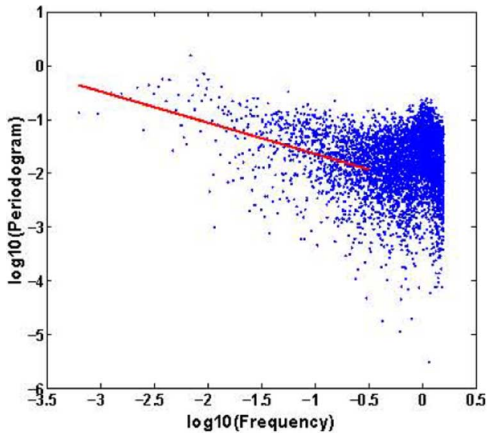

Fig. 4. Periodogram.

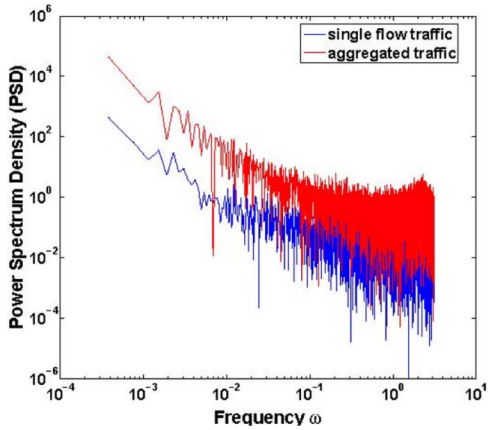

Fig. 5. PSD of aggregated traffic verse PSD of single-flow traffic.

m-aggregated time sequence $X^{(m)} = \{X^{(m)}(t), t \geq 1\}$ by summation of the original series X over nonoverlapping blocks of size m. Plot the variance of $X^{(m)}$ against m in the log-log scale. Then, a straight line with slope $(-\beta)$ greater than -1 can indicate long-range dependence, and corresponding Hurst parameter H can be given by $H = 1 - \beta/2$. The second method is the periodogram approach. The main procedure is to plot the periodogram in a log-log scale and calculate the slope of a regression line, which should be an estimate of $1 - 2H$.

C. LRD Behavior in Single-Node Traffic

Long-range dependence manifests itself either in time domain (power-law decay of the autocorrelation) or in spectral domain (power-law singularity of the spectral density at zero frequency). Here, we investigate the corresponding PSD in the mid-frequency range because the single-node traffic is expected to exhibit pseudo-LRD behavior if the characteristic index $\beta < 1$. Fig. 2 gives a rough estimate of PSD of the simulated single-user traffic based on a single trace measurement with 10 000 sampling points. PSD in Fig. 2 shows a trend of power-law decay especially in low-frequency domain, which indicates the possible presence of long-range dependence. To eliminate the deviation, Fig. 3 shows the averaged PSD based on the results from 50 trace measurements. Fig. 3 clearly shows the power law decaying PSD, which has a straight line with slope 0.8 in the mid-frequency range from 1 rad to the order of magnitude of 10^{-3} rad. According to the relationship between PSD and autocorrealtion, this observation indicates that the corresponding autocorrelation also exhibits power-law behavior. This is expected because according to the simulation settings, the correlation parameter β is less than 1. Under this condition, Proposition 2 points out that the autocorrelation of the single-node traffic obeys a power law in mid-frequency, which indicates pseudo-LRD traffic. To determine the Hurst parameter, we employ periodogram-based analysis. According to this approach, an estimate of $1 - 2H$ is given by computing the slope of a regression line of the periodogram plotted in log-log grid. Fig. 4 depicts the periodogram of a single trace used in Fig. 3. The periodogram plot shows a slope of 0.7376, yielding an estimate of H as 0.8683. The estimated H closely approximates the theoretical $H = 0.9$ according to Proposition 2.

D. LRD Behavior in Relay-Node Traffic

Next, we test the LRD of the traffic at a relay node. We assume the traversing probability is 1, which means each flow in the network is active all the time. The maximum number of flows the relay node can support is set to be 20. Fig. 5 compares the aggregated traffic at the relay node with single-flow traffic in terms of PSD. It can be seen that the PSD of the traffic at the relay node closely resembles that of the single-flow traffic except that the PSD of the aggregated traffic is 20 dB higher. From the modified periodogram depicted in Fig. 6, it can be noticed that the aggregated traffic has the same Hurst parameter as the single-flow traffic. These results are expected because according

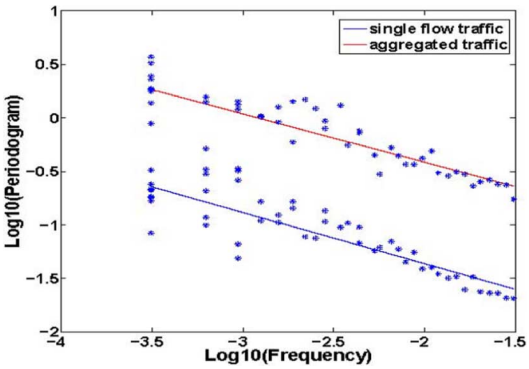

Fig. 6. Modified periodogram of aggregated traffic verse modified periodogram of single-flow traffic.

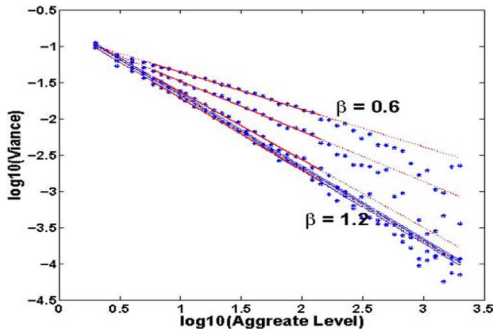

Fig. 7. Effects of mobility and spatial correlation on the traffic pattern.

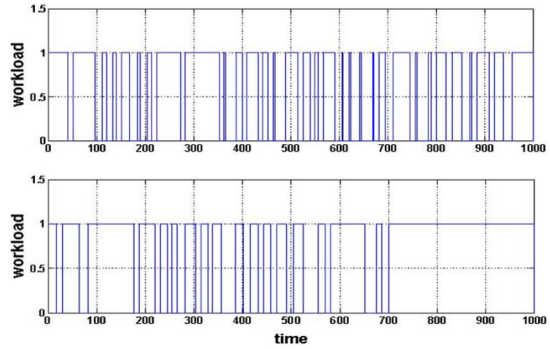

Fig. 8. Traffic load originating from a single node. *(top)* Exponentially distributed flight length. *(bottom)* Heavy-tail distributed flight length.

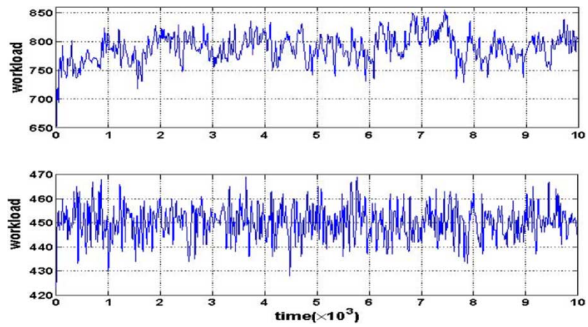

Fig. 9. Traffic load resulting from the aggregation of 20 traffic flows. *(top)* $\alpha = 1.2$. *(bottom)* $\alpha = 12$.

to Proposition 5, the traffic at the relay node has the scaled version of autocovariance of the single-flow traffic, and this suggests that the PSD of the aggregated traffic is only a shift of the PSD of single-flow traffic in log-log scale, thus also making the Hurst parameter unchanged.

E. Impact of Characteristic Index on Hurst Parameter

We now investigate the impact of characteristic index β on the autocorrelation function. Fig. 7 depicts the variance-time plot of the traffic trace under different correlation parameter β ranging from 0.5 to 1.2. It is seen that the variance-time plot is linear and shows a slope that is different from -1. The slope yields an estimate for $2H-2$. It can be seen in Fig. 7 that larger β yields the slope with smaller deviation from -1, which indicates smaller H and less bursty traffic. It can be also observed that when β becomes larger than 1, the variance-time curve overlaps with the straight line with slope of -1, which suggests that the traffic is nonbursty. The results are as expected because Proposition 2 points out that high mobility variability with small spatial correlation yields smaller β. This leads to hyperbolic autocorrelation function with larger Hurst parameter, thus indicating more bursty traffic.

F. Effect of Traffic Shaping Protocols on Burstiness Reduction

The objective of the traffic shaping protocols is to reduce the traffic burstiness. To investigate the protocol performance, we compare the traffic traces collected from two scenarios. The first one considers the sensor nodes programmed to follow exponentially distributed flight length. The second one considers the sensor nodes following heavy-tail flight length. Fig. 8 depicts a single-node traffic trace under the considered two scenarios, respectively. For the first scenario (upper figure), the ON period lengths are evenly distributed, which indicates smooth traffic. This is as expected because exponential distributed flight length leads to light-tail distributed ON period [e.g., see (47)], and this indicates SRD or nonbursty traffic. For the second scenario (lower figure), the ON period lengths exhibit high variance, which indicates bursty traffic. The effect can be explained by the hyperbolic file size induced by the highly variable flight length.

By using the proposed protocols, the burstiness reduction effects can be also seen in the relay-node traffic. Fig. 9 shows the significantly different traffic traces caused by two mobility patterns. Both patterns follow the same flight-length distribution as shown in (1) with different tail index α. In the first case (upper figure), all the nodes adopt the same tail index $\alpha = 1.2$, and the relay-node traffic exhibits low frequency variations, which indicates the LRD-like behavior and high intensity of bursts. In the second case (lower figure), all the nodes adopt the same tail index $\alpha = 12$, and the aggregated traffic on the relay node has oscillations mostly in high frequency, which is to be expected, because high frequency variations will correspond limited bursts.

G. Validating the ON/OFF *Model for Single-Node Traffic*

Next, we carried out the experiments in a large-sale simulated sensor network deployed in a large monitoring region. All the settings of this network are configured according to above-mentioned hybrid network scenario. The actual traffic traces are first collected from this network. Then, we synthesize traffic traces based on the proposed traffic model and show that the synthesized traffic fits the actual traffic. This strategy that utilizes the large-scale simulated sensor network to generate experimental

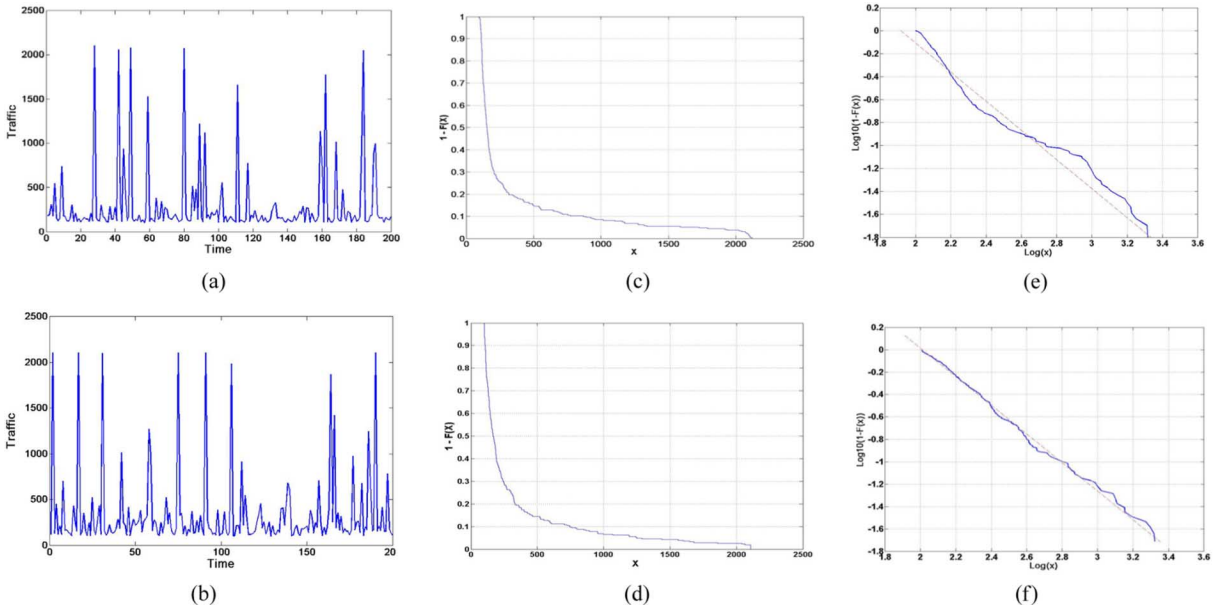

Fig. 10. (a) Actual single-user network traffic and corresponding (c) ccdf plot and (e) tail index estimate. (b) Synthesized traffic trace and corresponding (d) ccdf plot and (f) tail index estimate. Only one synthesized trace is shown.

traces for validating analytical results is widely used in sensor network research. Some works using this strategy include data compression analysis [5], [6], MAC protocol design [20], and packet traffic modeling [21].

The actual traffic is generated by a mobile agent, which moves around within an experiment region of 5000×5000. The measurements at each location in this region are generated according to the two-dimensional Gaussian random field with the power exponential correlation coefficient, zero mean, and 1 covariance. The static sensor nodes first discretize the continuous measurement by encoding it with one of the seven symbols. Each symbol corresponds to one of the seven regions including $(-\infty, -2.5)$, $[-2.5, -1.5)$, $[-1.5, -0.5)$, $[-0.5, 0.5)$, $[0.5, 1.5)$, $[1.5, 2.5)$, and $[2.5, \infty)$. Then, the static sensor node assembles five consecutive encoded measurements as an event and stores all the events locally. Next, the mobile agent initiates its movement according to the human mobility model—that is, for each movement, its actual traveled distance is drawn from the heavy-tailed distribution with $\alpha = 0.75$. After each movement, the mobile node retrieves the interested events from the closest static sensor node. In this case, the interested events at the current location are the new events that occur at the same time as the events the most frequently detected at the previous location, but have different values or encoded symbols.

In Fig. 10(a), we show the volume of the actual traffic measured during each transmission period. Since constant transmission rate is adopted, the traffic volume actually indicates the length of the transmission period. The corresponding ccdf and tail index estimate of the transmission periods are shown in Fig. 10(c) and (e), respectively. The tail index is estimated through linear regression in the log-log ccdf plot [Fig. 10(e)]. The linearity in this figure indicates that the actual traffic traces are indeed heavy-tail distributed. Fig. 10(b) depicts the synthesized traffic using the proposed ON/OFF model. The tail index γ_a of the proposed model is obtained through the tail index estimate of the actual traffic traces. We observe that the outlooks of the two traces are very similar, i.e., they are impulsive. We also plot the ccdf of synthesized traffic in Fig. 10(d), which shows the similar trend of the actual traffic in Fig. 10(c). In addition, the straight line in the tail index estimate plot [Fig. 10(f)] clearly shows that the synthesized traffic is heavy-tail distributed.

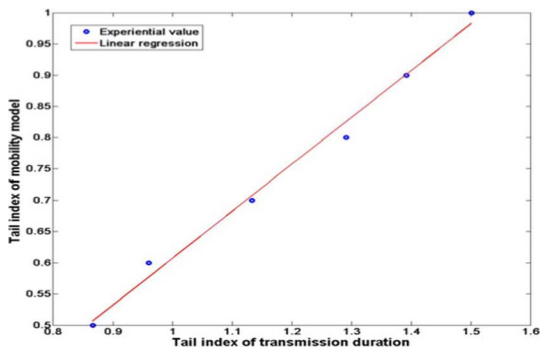

Fig. 11. Linear relationship between traffic trail index and mobility tail index.

Next, we measure the actual traffic, varying the node mobility behavior, i.e., varying the tail index α from 0.5 to 1. In Fig. 11, we plot the tail index of the flight (travel distance) traces versus the corresponding tail index of the actual traffic traces. The linearity in Fig. 11 indicates that as mobility variability increases, the traffic becomes burstier. To further confirm this observation, in Fig. 12, we plot the volume of the actual traffic measured under the scenarios with each transmission period. It is shown that the traffic becomes less impulsive or bursty as α decreases.

V. Conclusion

This paper proposed a novel traffic model for WSNs with mobile agents. This scheme captures the statistical patterns of the mobility and spatial correlation. It is shown that the intensity of the traffic burstiness or the Hurst parameter is completely determined by the mobility variability and the degree of the spatial correlation. More specifically, higher mobility variability and smaller spatial correlation could yield higher Hurst value, which

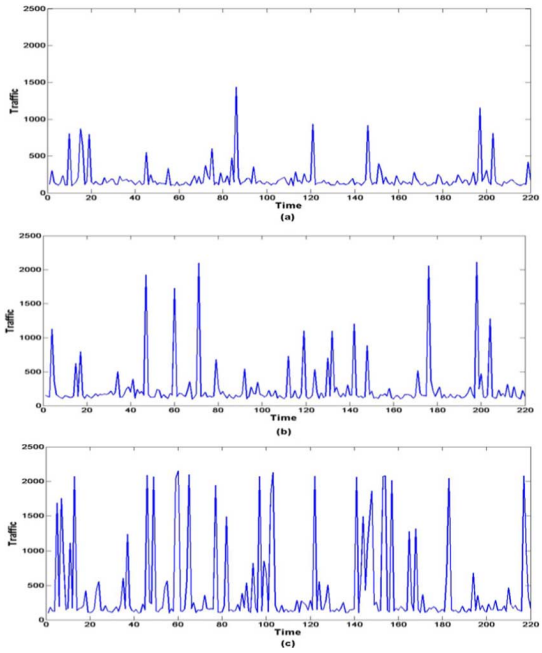

Fig. 12. Traffic under different mobility variability: (a) $\alpha = 1$. (b) $\alpha = 0.75$. (c) $\alpha = 0.5$.

indicates more bursty traffic. Conversely, smaller mobility variability and higher spatial correlation could lead to more smooth traffic. These findings have been exploited to design the traffic shaping protocols, which can facilitate the simple and effective resource-provisioning strategy by reducing the traffic burstiness through the adaptive coordination of node movement. The simulation results have been shown in close agreement between the theoretical propositions and the observed statistical properties.

Appendix A
Heavy-Tail Distribution

A random variable X has a heavy-tail distribution if its survival function follows

$$\bar{F}(x) = P(X > x) \to cx^{-\alpha}, \qquad \text{as } x \to \infty \tag{48}$$

where the symbol $\to$ indicates that the ratio of the left- and the right-hand side tends to 1. $0 < \alpha < 2$ is called tail index or shape parameter, and c is a positive constant. Heavy-tail distributed random variables have infinite variance for $0 < \alpha < 2$, and an unbounded mean for $0 < \alpha < 1$. The main characteristic of a heavy-tail distributed random variable is the extreme variability it exhibits. That is, heavy-tail distribution can give rise to very large values with nonnegligible probability. A frequently used heavy-tail distribution is Pareto distribution, whose survival function is given as

$$\bar{F}(x) = P(X > x) = \left(\frac{b}{x}\right)^{\alpha}, \qquad x > b \tag{49}$$

where $0 < \alpha < 2$ is tail index and b is called the location parameter, which is the minimum possible value of X.

In many practical applications, there is a natural upper bound that truncates the probability tail. For example, all data sets have finite size. In this case, truncated Pareto distribution is more appropriate for mathematical modeling. The truncated Pareto distribution can be expressed by

$$f(x) = \frac{\gamma x^{-(\gamma+1)}}{k_{\min}^{-\gamma} - k_{\max}^{-\gamma}}, \qquad k_{\min} < x < k_{\max} \tag{50}$$

where $k_{\min}(k_{\max}\})$ denotes the lower (upper) bounds. γ denotes the tail index.

Appendix B
Proof of Proposition 2

Proposition 1 shows the survival function of the ON period length follows power-law form with the tail index $\gamma_a = 2\beta$ in the region $k_1 < x < k_2$. In this case, the survival function can be characterized by Pareto distribution, which is given by

$$\bar{F}^*_{\tau_a}(x) = \left(\frac{k_1}{x}\right)^{\gamma_a}, \qquad x \in [k_1\ k_2]. \tag{51}$$

In addition, Proposition 1 points out if $x > k_2$, then the tail index is always larger than 2. This means the survival function in this region decays much faster than the heavy-tail distribution. Thus, exponential distribution can be used to approximate the survival function within the region $k_2 < x < k_3$. That is

$$\bar{F}^*_{\tau_a}(x) = \mu e^{-\lambda x}, \qquad x \in [k_2\ k_3]. \tag{52}$$

The exponent λ can be obtained by the exponent index function given by

$$\vartheta(x, \beta) = \frac{d \log \bar{F}_{\tau_a}(x)}{dx}. \tag{53}$$

Since the initial point of the exponential distribution is located at $(k_2, \bar{F}_{\tau_a}(k_2))$, then the parameters λ and μ can be given by

$$\lambda = \vartheta(k_2, \beta) = \frac{-\beta(\log e \ln 10)^{-1}\sqrt{2R^*}}{\sqrt{\pi e r^{-2}}\sigma(1-R^*)\ln(1-R^*)} \tag{54}$$

and

$$\mu = \exp\left(\frac{-2\beta(\log e \ln 10)^{-1}R^*}{(1-R^*)\ln(1-R^*)}\right) \times \left((-\ln(1-R^*))^{-1}\ln\left(\frac{t_{\max}^2}{t_{\max}^2 - k_1^2}\right)\right)^{\beta}. \tag{55}$$

Appendix C
Proof of Proposition 4

Based on the relationship between the PSD of a real-valued process and its autocorrelation, we obtain the autocovariance $C_X(t)$ based on the PSD given by

$$\begin{aligned} C_X(t) &= R_X(t) - E^2[X(t)] \\ &= 2\int_{0^+}^{\infty} S(f)\cos(2\pi f t)df \\ &= C_1\pi^{-1}t^{1-\gamma_a}\int_0^{\infty} x^{\gamma_a - 2}\cos(x)dx \\ &\quad + C_2\pi^{-1}t^{1-\gamma_b}\int_0^{\infty} x^{\gamma_b - 2}\cos(x)dx \\ &= A_1 t^{1-\gamma_a} + A_2 t^{1-\gamma_b} \end{aligned} \tag{56}$$

where A_1 and A_2 are some constants. The power-law form of autocovariance implies that the single-node traffic has the Hurst parameter

$$H = \frac{3 - \min(\gamma_a, \gamma_b)}{2} \approx \frac{3 - \min(2\beta, \gamma_b)}{2}. \quad (57)$$

Since $\beta < 1$ and $\beta_b > 2$, we obtain

$$H \approx \frac{3 - 2\beta}{2}. \quad (58)$$

REFERENCES

[1] I. F. Akyildiz and I. H. Kasimoglu, "Wireless sensor and actor networks: Research challenges," *Ad Hoc Netw.*, vol. 2, pp. 351–367, Oct. 2004.

[2] I. F. Akyildiz, W. Su, Y. Sankarasubramaniam, and E. Cayirci, "Wireless sensor networks: A survey," *Comput. Netw.*, vol. 4, no. 12, pp. 393–422, Mar. 2002.

[3] Z. Butler and D. Rus, "Event-based motion control for mobile-sensor network," *IEEE Pervasive Comput.*, vol. 2, no. 5, pp. 34–42, Oct.–Dec. 2003.

[4] T. M. Cover and J. A. Thoma, *Elements of Information Theory*, 1st ed. New York: Wiley, 1991.

[5] R. Cristescu, B. Beferull-Lozano, and M. Vetterli, "On network correlated data gathering," in *Proc. IEEE INFOCOM*, Hong Kong, China, Mar. 2004, pp. 2571–2582.

[6] R. Cristescu, B. Beferull-Lozano, and M. Vetterli, "Networked Slepian–Wolf: Theory, algorithms, and scaling laws," *IEEE Trans. Inf. Theory*, vol. 51, no. 12, pp. 4057–4073, Dec. 2005.

[7] R. Dahlhaus, "Efficient parameter estimation for self-similar processes," *Ann. Statist.*, vol. 17, pp. 1747–1766, 1989.

[8] I. Demirkol, F. Alagoz, H. Delic, and C. Ersoy, "Wireless sensor networks for intrusion detection: Packet traffic modeling," *IEEE Commun. Lett.*, vol. 10, no. 1, pp. 22–24, Jan. 2007.

[9] N. G. Duffield and N. O'Connell, "Large deviations and overflow probabilities for the general single-server queue, with application," *Math. Proc. Cambridge Philos. Soc.*, vol. 118, no. 2, pp. 363–375, 1995.

[10] V. Giordano, P. Ballal, F. Lewis, B. Turchiano, and J. Zhang, "Supervisory control of mobile sensor networks: Math formulation, simulation, and implementation," *IEEE Trans. Syst., Man, Cybern. B, Cybern.*, vol. 36, no. 4, pp. 806–819, Aug. 2006.

[11] M. Grossglauser and J.-C. Bolot, "On the relevance of long-range dependence in network traffic," *IEEE/ACM Trans. Netw.*, vol. 7, no. 5, pp. 629–640, Oct. 1999.

[12] C. L. Hwang and S. Q. Li, "On input state space reduction and buffer noneffective region," in *Proc. IEEE INFOCOM*, Toronto, ON, Canada, 1994, pp. 1018–1028.

[13] W. E. Leland, M. S. Taqqu, W. Willinger, and D. V. Wilson, "On the self similar nature of ethernet traffic (extended version)," *IEEE/ACM Trans. Netw.*, vol. 2, no. 1, pp. 1–15, Feb. 1994.

[14] S. B. Lowen and M. C. Teich, *Fractal-Based Point Processes*, 1st ed. New York: Wiley, 2005.

[15] G. Messier and I. Finvers, "Traffic models for medical wireless sensor networks," *IEEE Commun. Lett.*, vol. 11, no. 1, pp. 13–15, Jan. 2007.

[16] I. Norros, "Large deviations and overflow probabilities for the general single-server queue with application," *Queueing Syst.*, vol. 16, pp. 387–396, 1994.

[17] E. Petriu, T. Whalen, R. Abielmona, and A. Stewart, "Robotic sensor agents: A new generation of intelligent agents for complex environment monitoring," *IEEE Instrum. Meas. Mag.*, vol. 7, no. 3, pp. 46–51, Sep. 2004.

[18] I. Rhee, M. Shin, S. Hong, K. Lee, and S. Chong, "On the Levy-walk nature of human mobility," in *Proc. IEEE INFOCOM*, 2008, pp. 924–932.

[19] M. C. Vuran, O. B. Akan, and I. F. Akyildiz, "Spatio-temporal correlation: Theory and applications for wireless sensor networks," *Comput. Netw.*, vol. 45, no. 3, pp. 245–261, 2006.

[20] M. C. Vuran and I. F. Akyildiz, "Spatial correlation-based collaborative medium access control in wireless sensor networks," *IEEE/ACM Trans. Netw.*, vol. 14, no. 2, pp. 316–329, Apr. 2006.

[21] W. Willinger, V. Paxson, and M. S. Taqqu, "Self-Similarity and heavy-tails: Structural modeling of network traffic," in *A Practical Guide to Heavy Tails: Statistical Techniques and Applications*, R. Adler, R. Feldman, and M. S. Taqqu, Eds. Cambridge, MA: Birkhauser, 1998.

Pu Wang (S'10) received the B.S. degree in electrical engineering from Beijing Institute of Technology (BIT), Beijing, China, in 2003, and the M.Eng. degree in computer engineering from Memorial University of Newfoundland, St. John's, NL, Canada, in 2007, and is currently pursuing the Ph.D. degree in electrical and computer engineering under the supervision of Prof. Ian F. Akyildiz.

He is a Graduate Research Assistant with the Broadband Wireless Networking Laboratory (BWN Lab), School of Electrical and Computer Engineering, Georgia Institute of Technology, Atlanta. His current research interests are in wireless sensor networks, cognitive radio networks, and traffic engineering in large-scale networks.

Ian F. Akyildiz (M'86–SM'89–F'96) received the B.S., M.S., and Ph.D. degrees in computer engineering from the University of Erlangen-Nuernberg, Nuremberg, Germany, in 1978, 1981, and 1984, respectively.

Currently, he is the Ken Byers Distinguished Chair Professor with the School of Electrical and Computer Engineering (ECE), Georgia Institute of Technology (Georgia Tech), Atlanta, and Director of the Broadband Wireless Networking Laboratory. Since June 2008, he has been an Honorary Professor with the School of Electrical Engineering, Universitat Politecnico de Catalunya, Barcelona, Spain. He is the Editor-in-Chief of *Computer Networks* as well as the founding Editor-in-Chief of *Ad Hoc Networks* and *Physical Communication*. His current research interests are in cognitive radio networks, wireless sensor networks, wireless mesh networks, and nanocommunications.

Prof. Akyildiz has been a Fellow of the Association for Computing Machinery (ACM) since 1996. He received the "Don Federico Santa Maria Medal" for his services to the Universidad of Federico Santa Maria, Valparaíso, Chile, in 1986. From 1989 to 1998, he served as a National Lecturer for ACM and received the ACM Outstanding Distinguished Lecturer Award in 1994. He received the 1997 IEEE Leonard G. Abraham Prize Award (IEEE Communications Society) for his paper titled "Multimedia Group Synchronization Protocols for Integrated Services Architectures," published in the IEEE JOURNAL OF SELECTED AREAS IN COMMUNICATIONS in January 1996. He received the 2002 IEEE Harry M. Goode Memorial Award (IEEE Computer Society) with the citation "for significant and pioneering contributions to advanced architectures and protocols for wireless and satellite networking." He received the 2003 IEEE Best Tutorial Award (IEEE Communication Society) for his paper titled "A Survey on Sensor Networks," published in *IEEE Communications Magazine* in August 2002. He also received the 2003 ACM SIGMOBILE Outstanding Contribution Award with the citation "for pioneering contributions in the area of mobility and resource management for wireless communication networks." He received the 2004 Georgia Tech Faculty Research Author Award for his "outstanding record of publications of papers between 1999–2003." He received the 2005 Distinguished Faculty Achievement Award from the School of ECE, Georgia Tech. He received Georgia Tech Outstanding Doctoral Thesis Advisor Award for his 20+ years of service and dedication to Georgia Tech and for producing outstanding Ph.D. students. He received the 2009 ECE Distinguished Mentor Award by the Georgia Tech School of Electrical and Computer Engineering Faculty Honors Committee. He received the 2010 IEEE Communications Society Ad Hoc and Sensor Networks Technical Committee (AHSN TC) Technical Recognition Award. He also received the IEEE Computer Society W. Wallace McDowell Award.